arXiv:astro-ph/0403630v1 26 Mar 2004

A three-dimensional calculation of atmospheric neutrinos

G.D. Barr[1], T.K. Gaisser[2], P. Lipari[3], S. Robbins[1], T. Stanev[2]

[1] *Department of Physics, University of Oxford,*
Denys Wilkinson Building, Keble Road, Oxford, UK, OX1 3RH

[2] *Bartol Research Institute, University of Delaware,*
Newark, Delaware, USA 19716

[3] *Dipartmento di Fisica, Universitá di Roma (La Sapienza)*
and INFN, Sezione di Roma, P. A. Moro 2, I-00185 Roma, Italy

February 2, 2008

Abstract

A Monte-Carlo calculation of the atmospheric neutrino fluxes [1, 2] has been extended to take account of the three-dimensional (3D) nature of the problem, including the bending of secondary particles in the geomagnetic field. Emphasis has been placed on minimizing the approximations when introducing the 3D considerations. In this paper, we describe the techniques used and quantify the effects of the small approximations which remain. We compare 3D and 1D calculations using the same physics input in order to evaluate the conditions under which the 3D calculation is required and when the considerably simpler 1D calculation is adequate. We find that the 1D and 3D results are essentially identical for $E_\nu > 5$ GeV except for small effects in the azimuthal distributions due to bending of the secondary muon by the geomagnetic field during their propagation in the atmosphere.

1 Introduction

The hypothesis that neutrino oscillations are observed in the fluxes of muon-neutrinos produced from cosmic ray interactions in the upper atmosphere [3, 4] has held up well in analysis of high statistics data from Super-Kamiokande [5] and at other experiments [6, 7]. What was once called an 'atmospheric neutrino anomaly' is now accepted as an established demonstration of neutrino mass [8]. The atmospheric neutrino oscillation result is obtained by comparing measured fluxes of muon- and electron-neutrinos in underground detectors with computations based on modeling hadronic interactions in the atmosphere over the surface of the globe. The angular dependence of the muon to electron ratio and its energy dependence probe a range of nearly 5 orders of magnitude in L/E. Deviations

from the expected behavior, in particular a deficit of muon neutrinos, point to oscillations in the $\nu_\mu \leftrightarrow \nu_\tau$ sector.

Until recently, only one-dimensional (1D) calculations of the neutrino flux have been used to infer oscillation parameters from the data. In the 1D approximation, all interactions and decay products follow the direction of the incident cosmic-ray particle that produced them. This approximation simplified the problem so that it could be tackled on computers of that era. Even now, a calculation which removes this limitation requires careful choice of technique and considerable computer time to be successful.

It is known that the 1D approximation neglects a geometrical effect which dramatically changes the predicted zenith angle distributions at low energies [9] (see figure 3). However, in oscillation studies, the neutrino spectrum is cut at low energies by detector acceptance, smeared due to the experimental determination of the neutrino direction and weighted by the neutrino cross section which increases (approximately linearly) with neutrino energy. These effects combine to reduce the importance of a full three-dimensional (3D) calculation to the point where its effect on the extraction of oscillation parameters is expected to be slight even though it considerably complicates the calculation and data analysis procedure. Nevertheless, in view of the importance of the result, it is essential to use fully three-dimensional calculations for interpretation of the data to infer the oscillation parameters.

In this paper we extend our original 1D calculation [1, 2] to include a full 3D treatment of showers across the whole surface of the globe. Our goal has been to make a code that is sufficiently fast to be able to investigate systematically the choices used in making an accurate calculation without the 1D approximation. We compare the 3D and 1D calculations in detail (along with various intermediate steps) in order to display the origin of characteristic features of the 3D calculation. We also identify the situations in which the 1D results adequately approximate those of the 3D calculation. In particular, we will identify the neutrino energy above which, 1D calculations can still be used.

This paper deals with the technical aspects of moving from a 1D to a 3D calculation. In §2 we describe the steps in our calculation in the context of previous 3D calculations. In §3 we present and discuss comparisons between 1D and 3D results as a function of neutrino energy and direction (zenith and azimuth). We also summarize some important technical aspects of a 3D calculation as well as the differences between 3D and 1D results in §3. Comparison of our calculated neutrino fluxes with others and evaluation of the larger uncertainties caused by different choices of hadronic models and differences among measurements of the primary cosmic-ray spectrum will be given in a later publication.

2 Overview of calculation

The neutrino flux is a convolution of the primary cosmic ray flux with the neutrino yields from interactions of the cosmic rays in the atmosphere. In general, the directional dependence of the flux at the detector is obtained by generating showers with random positions over the globe and collecting the neutrinos that pass through the detector. See Ref. [10] for a review.

As a consequence of the geomagnetic field, the primary cosmic-ray spectrum incident

on the atmosphere depends on location. In a 1D calculation, the assumption is that all secondaries follow the direction of the primary particle that initiated the cascade in which they were produced. In the 1D calculation, therefore, the geomagnetic field can be accounted for simply by evaluating the geomagnetic cutoff at each grid point on the globe for the single direction that points toward the detector. Moreover, the 1D calculation is extremely efficient because only cascades pointed at the detector need be generated. In reality, however, the secondaries deviate from the direction of the primaries. In a 3D calculation, therefore, one must sample incident particles from all directions at each point on the globe. The efficiency of a fully 3D calculation then is of order $A/R_\oplus^2 \sim 10^{-10}$, where A is the projected area of the detector and $R_\oplus = 6372$ km the radius of the Earth. Because the center of the geomagnetic dipole is offset from the center of the Earth, and because the field is not an exact dipole, any symmetry technique for making the calculation manageable involves an approximation that is difficult to quantify.

Deviations of cascade particles from the direction of the primary have two sources. First is the transverse momentum characteristic of hadronic interactions (~ 300 MeV/c for pions) and the decay processes such as $\pi^+ \to \nu_\mu \mu^+$ followed by $\mu^+ \to e^+ \nu_e \overline{\nu}_\mu$ in which the neutrinos are produced. The scale of this deviation is set by pion production as

$$\frac{\langle p_T \rangle}{E_\pi} \sim \frac{300 \text{ MeV}}{E_\pi} \sim \frac{0.1}{E_\nu \text{ GeV}} \text{ radians.} \quad (1)$$

Characteristic 3D effects are therefore most important for neutrinos with sub-GeV energies.

In addition, there is a second source of deviation from the direction of the primary, which is the bending of muons in the geomagnetic field. In this case, because gyro-radius and decay length have opposite dependence on energy, the deviation is independent of energy and is typically of order 3°. The muon decay length is $\gamma\, c\, \tau_\mu \approx 6.2\,\text{km} \times E_\mu(\text{GeV})$ compared to typical production altitudes of 15 km, so only muons with several GeV and above begin to hit the ground before decay. This deviation from the 1D approximation therefore remains important up to high energy, particularly for large zenith angles where higher energy muons decay before reaching the ground.

Bending of primary cosmic-rays before they interact, as well as energy loss of muons and protons in the atmosphere must also be accounted for.

2.1 Survey of 3D neutrino flux calculations

Wentz et. al. [11] give a comprehensive summary of calculations of the neutrino flux, both 1D and 3D. Here we comment on 3D calculations, noting technical assumptions and approximations that have been made by the authors for comparison with our approach.

Battistoni et al. [12] made the first calculation showing the characteristic enhancement of low-energy neutrinos near the horizontal. The calculation was updated [13] with emphasis on use of the FLUKA interaction model [14]. The calculation ignores the geomagnetic field for all tracking within the atmosphere. This approximation allows the shower to be developed at an arbitrary position on the globe, then moved such that one of the neutrinos hits the detector. The cutoff energy (see below) is checked after the

location of the primary is fixed and the event rejected if the primary is below the cut-off rigidity. This procedure is efficient because each cascade has a high probability of generating a neutrino that is used.

Lipari [9, 15] performed a 3D calculation in which the particles were injected over the entire Earth's atmosphere. The detector is represented by a region of 1/5 the surface of the Earth. The paper emphasizes that not only bending of muons but also bending of protons in the geomagnetic field is important.

Honda et. al. [16] use a dipole magnetic field approximation which allows them to invoke the symmetry in the geomagnetic longitude to increase the collection efficiency at the detector. Many details of the consequences on the azimuthal differences introduced by the 3D calculation and of the path length distributions are addressed in this paper.

Tserkovnyak et al. [17] do a full 3D simulation similar to our own with an enlarged rectangular detector $10^\circ \times 40^\circ$ with the narrow direction aligned with magnetic north. This corresponds to an effective detector area of about 1% of the surface area of the Earth. While they use a large surface area, Tserkovnyak et al. point out that it is important not to enlarge the vertical dimension of the detector. Doing so tends to wash out the enhancement near the horizon.

Wentz et al. [11] also do a full 3D simulation using the CORSIKA simulation package [18]. Calculation of neutrinos from below is done by injecting primaries over the whole Earth and collecting neutrinos that pass within a circle of radius 1000 km of Super-Kamiokande. Downward neutrinos were calculated from locally injected primaries.

Liu et al. [19] inject particles over an injection sphere at 2000 km above the surface of the Earth. They then calculate the neutrino fluxes averaged over all azimuth in three bins of geomagnetic latitude. For comparison with Super-K they use a spherical section 15 degrees wide in latitude by 30 degrees in longitude.

With one exception, all 3D calculations (including ours) start by injecting particles near the top of the Earth's atmosphere. They then use backtracking, as described below, to check whether the chosen energy and direction of a particle is on an allowed trajectory, rejecting those that are not. Playskin [20] has attempted a much more ambitious calculation. He injects particles at $10 \times R_\oplus$ and follows their trajectories to see which ones interact in the Earth's atmosphere, presumably a tiny fraction of the total. The results of this calculation differ significantly from others for reasons that have so far not been well-understood.

Favier et al. [21] use an injection sphere at 380 km and calculate the flux in 3 zones of geomagnetic latitude. For comparison with Super-K they average over all azimuth within a band of geomagnetic latitude centered on the detector. They check by comparing to the flux limited to ± 30 degrees in longitude about the location of Super-K. A significant aspect of this paper is a comparison of the proton spectrum at the injection sphere obtained with the backtracking method with that obtained by injecting particles at 20 $R_\oplus$. The two methods agree, including reproduction of the "second spectrum" [22], thus giving a nice empirical confirmation of the backtracking method.

The diversity of techniques and results among the 3D calculations arises in part because of the difficulty of the computational problem. Detectors are small compared to the size of the Earth, and there is no symmetry to the problem which can be invoked without introducing some uncertainty. The emphasis of the current study is first, to provide a fast

code which can be run in many different configurations to investigate the importance of changes in the parameters and approximations used and second, to be accurate, by which we mean that the calculation should involve no approximations which affect the results by more than a few percent.

2.2 Details of this calculation

The calculation proceeds by running Monte-Carlo simulations of the interactions of the primary cosmic rays with the atmosphere. Separate runs are performed at fixed primary energies, prearranged in logarithmic steps in energy, 10 energies per decade from 1 GeV to 10 TeV. The separate runs allow the details of the primary flux and of the effects of the solar wind to be inserted at a later step when the runs are combined. In this way different primary spectra and different solar epochs can be treated without re-running the full shower simulation. The statistics of each run is determined by accumulating a fixed number of neutrinos.

The Earth is assumed to be a sphere of radius $R_\oplus = 6372$ km. Primaries are generated with random positions and angles on the injection sphere which is at a radius of $r = R_\oplus + 80$ km. Each primary which produces at least one neutrino in the detector is then subjected to the cutoff calculation (see below) which takes account of the effect of the Earth's magnetic field on the primary cosmic rays.

The superposition approximation is used to treat primary nuclei, i.e. the interaction of a projectile nucleus of mass A and total energy E is assumed to be equivalent to the sum of A individual nucleons interacting on the target air nucleus individually, each with energy E/A. Three runs are generated at each primary energy: with free primary protons; with bound primary protons; with bound primary neutrons. This is so that both bound protons and bound neutrons can be propagated in the Earth's magnetic field as if they were included in a nucleus with $A/Z = 2$.

The effect of the geomagnetic field on the interacting cosmic rays is included by applying the cutoff using the back-tracing technique. Consider a point A far from Earth where the flux is assumed to be isotropic. For each valid cosmic ray trajectory from point A to a point B on the injection sphere (radius $R_\oplus + 80$ km), Liouville's theorem assures that, since the phase space density at A is isotropic, then the phase space density at B, near the Earth is also locally isotropic around the direction of the trajectory.

The technique is to select the particle on the injection sphere isotropically and then backtrack it from B to A to see if it is indeed on a valid trajectory – i.e. that it projects back to a place far from the Earth. A trajectory is considered valid when the particle propagates to a distance of 30 $R_\oplus$ with a total path length shorter than $300R_\oplus$ without hitting the Earth. If this is true, then the neutrino is accepted. If the primary particle spirals back and either remains in the vicinity of the Earth or hits the Earth itself, then its neutrino is discarded.

During the backtracking process, it is important to use an adjustable step size depending on the local radius of curvature and the variation of the Earth's magnetic field; otherwise the calculation takes a long time or is inaccurate. In the present calculation, the step size adjusts itself by a factor of up to 100 along a particle trajectory. The NASA parameterizations of the Earth's magnetic field [23] have been used.

If a particle trajectory loops into the atmosphere and back out, then one of the conditions for Liouville's theorem is no longer satisfied because the particle may lose energy or interact. In fact, interactions of protons skimming the atmosphere produce albedo protons that can be below the local geomagnetic cutoff. This is the source of the "second spectrum" measured in detail by AMS [22]. In a 1D calculation, this cannot happen by definition – once the particle has started to interact with the atmosphere, all its progeny follow in a straight line (towards the detector) and all cosmic rays produced in the Earth's atmosphere are accounted for. In the 3D calculation we track all particles out to a sphere at radius $R_\oplus + 400$ km. Those which loop back before reaching this radius and interact are included, but the small number of secondary particles which spiral above this are lost. The effect of this loss is small because the second spectrum itself has a relatively low intensity [24].

Tracking within the atmosphere is carried out with a separate algorithm; the center of the Earth is the origin of our global coordinate system. The injection point of each primary is defined in this global coordinate system; then all points within a cascade are tracked relative to that starting point so as not to lose accuracy by combining large and small numbers. Double precision is used throughout. Whenever a neutrino is generated, we return to the global coordinate system to track the neutrino through the Earth.

Stepping is done for a fixed length $d\ell$ along the trajectory of each particle ($d\ell = 300$ m) except for kinetic energy below 200 MeV where energy loss is large or altitudes below 10 km where the atmospheric density is high (for which $d\ell = 30$ m). At the end of each track step, the local zenith angle is recalculated to take account of curvature of the Earth. From the altitude at the beginning and end of each step, the local atmospheric density and hence dx (in g/cm^2) is computed. For the present paper, the US standard atmosphere model is used over the entire surface of the Earth to obtain the variation of density with altitude. This is a good average of a more detailed model which includes seasonal and latitude dependent effects which is currently being implemented. The calculation neglects the elevation of the land masses and treats the surface of the Earth as being at sea level over the whole surface. (Detectors, however, are assigned their actual altitude.)

Charged particles bend in the magnetic field as they are tracked through the atmosphere. An internal proper-time clock is maintained for unstable particles to determine their decay point. Likewise, interacting particles are tracked until they have passed through the appropriate thickness of atmosphere at which point they interact. For pions and kaons, decay and interaction are competing processes, and the choice is made based on a comparison of the randomly chosen interaction and decay lengths.

The decay and interaction generators are modular in this code, so they can be plugged in and out in any combination. For the investigations in this paper, we use the interaction generator TARGET version 2.1 [25].

The results we present in this paper are obtained with the primary cosmic ray flux used by Agrawal et al [2]. Compared to the newer data sets this representation of the primary spectrum has a lower proton flux then was measured by AMS [26] and BESS [27] below 50 GeV, but higher then the ones measured by other experiments [28]. Another feature of this primary spectrum is that the all-nucleon flux has a flatter energy dependence at high energy than fits including the AMS and BESS data would give. How the primary spectrum extrapolates to high energy will be important for extension of the neutrino flux

into the TeV region.

In the 3D calculation, particles are injected across the entire globe and most neutrinos miss the detector and are not used to compute the flux. It is this reason why there is a huge step in complexity between a 1D and a 3D computation. To save computer time, a detector which is many times larger than the real detector is used in the simulation. Tuning the shape and size of the detector is crucial for a successful calculation. Following the advice from Ref. [17], we use a "flat" detector (i.e. a section from a spherical shell with curvature given by the sum of the radius of the Earth and the detector altitude). The difficulty with any other choice is that any significant enlargement in the vertical direction causes the detector to either poke out the top of the atmosphere or be so deep that the effects of the 3D geometry are not correctly represented. The question of how large the artificial detector in the calculation can be made, without introducing excessive inaccuracies, is addressed later in this paper. We employ a circular shape with radius 500 km, centered on the detector. Averaging of the neutrino flux over this distance introduces less than 0.5% bias in the results.

A further difficulty with using a truly flat detector is that the cross sectional area changes as a function of the zenith angle of the neutrino (θ_z), and vanishes for horizontal directions. This effect can be solved in the 1D case by generating primaries with a flat zenith angle distribution (θ_p). Since, for a 1D calculation, the primary direction is equal to the neutrino direction by definition, this correctly removes the effect of the changing cross section of a flat detector. (Another viewpoint is that the detector in a 1D calculation is simply a point, so the flatness issue never arises). In the 3D calculation, $\theta_p \neq \theta_z$ in general and the flat detector problem has to be addressed by introducing weights. There are two choices which have both been tried and give consistent results: (1) Generate particles in the atmosphere in the "natural" way, i.e. proportional to $\cos\theta_p$, and when each neutrino strikes the detector, it receives a weight of $1/\cos\theta_z$ to compensate for the reduced cross section; (2) generate particles isotropically (uniformly in $\cos\theta_p$) and weight each neutrino which strikes the detector by $\cos\theta_p/\cos\theta_z$. The second method has the advantage that in the limit of high neutrino energy where the 3D calculation generates essentially collinear showers, the technique tends to the 1D technique and the weight tends to unity. The second method is used in the calculations presented in this paper.

Both methods have the drawback that as the neutrino direction approaches the horizon the weights diverge. This reflects that fact that the probability of counting such an event in the Monte-Carlo tends to zero. This can lead to large fluctuations in the flux computed near the horizon, a feature which is unacceptable for use in experimental analysis of underground detector data to extract neutrino oscillation parameters. We have studied various techniques for avoiding large fluctuations [29] and have adopted a 'binlet' weighting scheme for this calculation. As each neutrino arrives at the flat detector, a bin in $\cos\theta_z$ is assigned to it. All neutrinos which enter this bin are assigned the weight given by the value of $\cos\theta_z$ at the center of the bin rather than at the individual value for each neutrino. It is important to use narrow bins for this to avoid bias, hence the name 'binlet'. For the present analysis, 80 'binlets' are used in the range $-1 < \cos\theta_z < 1$, so the maximum variation in weights is slightly less than 1:80. Further details of this and other viable techniques are discussed in Ref. [29].

To perform the 'binlet'-weighting, a special histogramming package was written. This

also allows the squares of the weights to be accumulated for computation of the Monte-Carlo statistical error on each point. These errors are shown on the figures in this paper.

To verify the functioning of the 3D calculation chain, we replaced the hadron production generator by a simplistic model which generated a neutrino with a fixed angle α to the primary, instantly at the injection sphere where the primaries were injected. This is shown in figure 1 for various different injection heights, compared with analytic formulae from Ref. [9]. The figure illustrates the basic expectations of the 3D geometric effects - a sharp enhancement near the horizon and a small reduction in flux near vertical. The effects increase strongly with increasing α and are therefore expected to be largest for low neutrino energy where interaction and decay of particles causes the largest angular change between primary and neutrino directions.

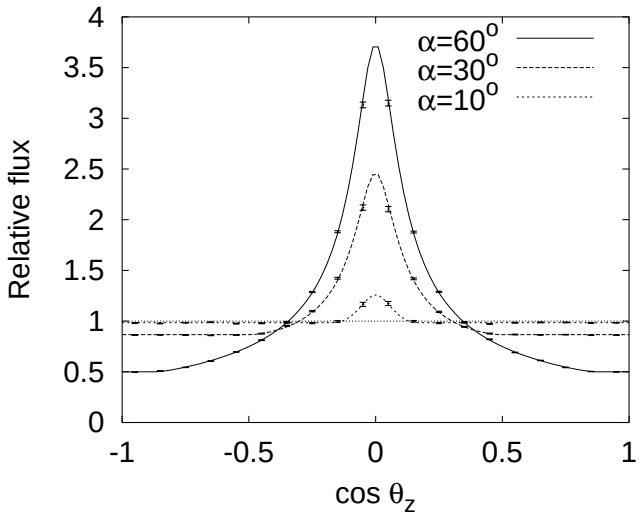

Figure 1: Comparison between a test Monte-Carlo calculation (points) which introduces a single bend through an angle α at an altitude of h and an analytic calculation from [9] (lines) for different values of $\alpha = 10°$, $30°$ and $60°$. These curves show the basic features of a 3D calculation (see text).

3 Results

The three dimensional simulation proceeds by running at each energy until about 1.2 million neutrinos hit the detector (or until one million primaries have been generated). The latter limit only occurs at low energy. All neutrinos passing within a circle of radius 500 km centered on the detector location are accepted. The calculation has been done so far at the site of the Super Kamiokande detector (Kamioka, Japan; Lat: 36.42 N, Lon: 137.310 E, Alt: 372 m) and at two adjacent northern latitude sites, Soudan-2/MINOS (Soudan, Minnesota, USA; Lat: 47.822 N, Lon: 267.752 E, Alt: Sea level) and SNO (Sudbury, Ontario, Canada; Lat: 46.475 N, Lon: 278.632 E, Alt: -1.7 km).

Several modes of operation of the code are available to allow the change between a full 3D calculation and a 1D calculation to be made in steps in the same program.

- **3D** The full 3-dimensional treatment.
- **NM** The 3D treatment, but with bending of particles within the atmosphere turned off.
- **pseudo-1D** All transverse momenta are set to zero and there is no bending within the atmosphere. Particles are still generated in all directions over the entire globe and the details of the flat detector in three dimensions are still included. In principle, running in this mode should produce results in agreement with a 1D calculation, allowing us to test the integrity of the 3D cascade code in the absence of 3D effects.
- **1D** It is also possible to operate the 3D program in a classical 1D mode, in which there is no p_T, no magnetic field and only trajectories pointing directly at the detector center are generated. This differs from the pseudo-1D calculation in that the weighting schemes are not needed.
- **original-1D** The original code from Ref. [2] was used with the 2.1 version of target.

Comparisons among these five calculations are shown in the following part of the paper. To summarize, original-1D, 1D and pseudo-1D agree with each other in all distributions except for statistical fluctuations in the pseudo-1D. This agreement is important as it checks the correct realization of the weighting procedures in the pseudo-1D calculation, which are identical to those in the 3D. Generally NM agrees with either the 3D or the 1D runs as described below and gives insight into the origin of the differences between 1- and 3-dimensional calculations.

The angle integrated fluxes of neutrinos and antineutrinos at Kamioka and Soudan are compared with each other in figure 2. The fluxes at SNO are similar to those at Soudan. The 3D and original-1D fluxes are plotted. All three 1D calculations are identical on this scale over the whole energy range between 0.1 and 10 GeV. The fluxes are before any oscillations, and the calculations were performed in the epoch of solar minimum. The large difference in fluxes between Kamioka and Soudan is due to the difference in local cutoffs; Kamioka is near the geomagnetic equator where the downward cutoffs are large (around 20 GeV, but direction dependent) while Soudan is near the geomagnetic pole where the downward cutoffs are only a few GeV and more low energy primaries get through. This plot shows that in changing from 1D to 3D calculation, there is a $\sim 3\%$ increase in 3D sub-GeV angle-averaged fluxes. For $E_\nu > 1$ GeV, the angle-integrated fluxes from the 3D and 1D calculations are identical within statistical differences of about a per cent.

Figure 3 compares the zenith angle distributions at Kamioka (solar minimum) obtained with the 3D and pseudo-1D modes for various energy ranges. It illustrates the second essential feature of the change from 1D to 3D calculation, which was first noted by Battistoni et al.[12]: At low energy, the geometrical effect causes an enhancement in 3D-fluxes near the horizon and a smaller depletion of fluxes near the zenith. The effect

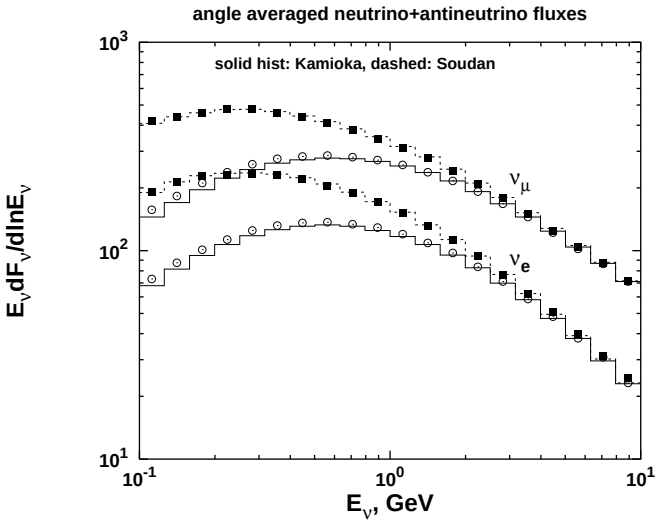

Figure 2: Comparison of 3D to 1D calculation of the angle averaged fluxes at Kamioka and Soudan. The $(\nu_\mu + \overline{\nu}_\mu)$ and $(\nu_e + \overline{\nu}_e)$ fluxes are plotted for the 3D calculation (points) and the 1D calculation (lines).

decreases as the neutrino energy increases. At higher energies, the two distributions become more similar. The broad peak in the high-energy flux is common to 3D and 1D calculations. It is caused by a combination of two effects: decay of charged pions is enhanced at large angles relative to hadronic interaction ($\sec\theta$ effect), and higher-energy muons at larger zenith angle can still decay before reaching the ground.

At neutrino energies exceeding 5 GeV the two zenith angle distributions become identical. There are, however, still some differences in the azimuthal distributions, which will be discussed below.

3.1 Ratios of fluxes

Figure 4 shows the ratio R of muon-type to electron-type neutrino fluxes as a function of neutrino energy for the 1D, NM and 3D calculations. The ratio is calculated using $\nu + \frac{1}{2}\bar{\nu}$ as an approximate way to account for the difference in interaction cross-section between neutrinos and antineutrinos. The main features of the ratio may be understood simply by counting the three neutrinos (two muon-type and one electron-type) associated with each muon in the atmosphere and noting that the kinematics works so that each neutrino has about the same energy. This gives $R = 2$. At higher energies R increases as muons begin to reach the ground before decaying. There are no changes in the flavor ratio between 1D and 3D calculations. The fluctuation seen in the zenith angle distribution near the horizon for the NM case is within statistics.

Figure 5 shows the ratio of neutrinos to antineutrinos as a function of energy and zenith angle. At low energy, the simple neutrino counting argument from above gives an expected ratio of 1. At higher energies where muons hit the ground, the ratios increase a little to reflect the μ^+/μ^- ratio of about 1.25 from hadron production. Kaons play

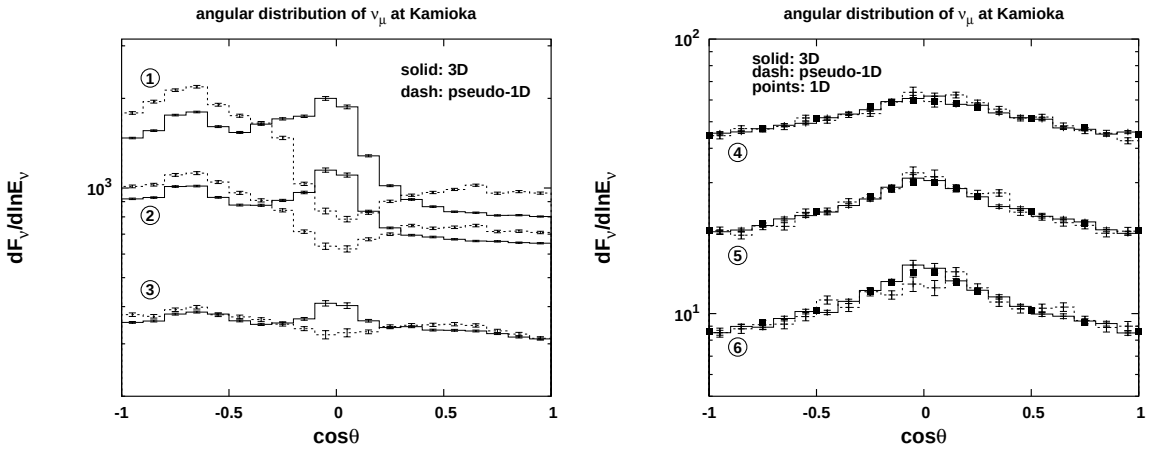

Figure 3: Zenith angle distributions of ν_μ at Kamioka for six different energy ranges. The full-line histograms are the 3D calculation and the dashed histograms are the pseudo-1D calculation. The energy ranges in the left hand panel are: 1) 100–158 MeV, 2) 250–400 MeV, and 3) 630 MeV–1 GeV. In the right hand panel we show the angular distribution for 4) 2.50–4.0 GeV, 5) 4.0–6.3 GeV, and 6) 6.3–10 GeV. The right panel also contains the angular distributions calculated with Bartol's original code (points).

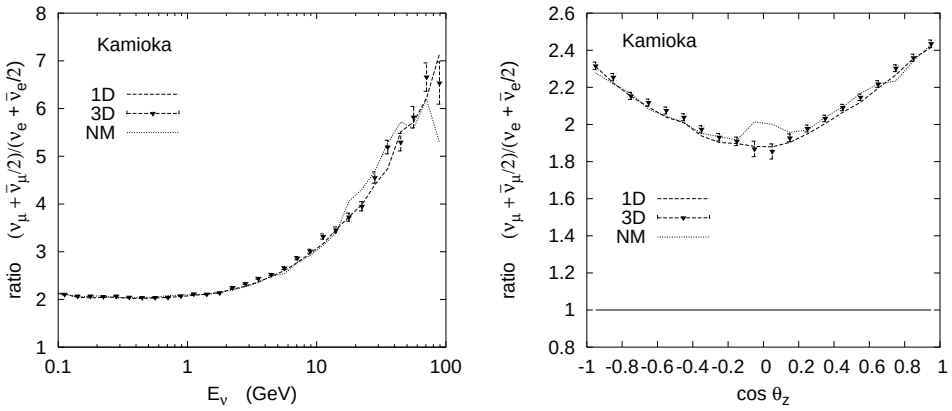

Figure 4: Ratio of muon-like to electron-like neutrinos as a function of (a) E_ν and (b) zenith angle (for $E_\nu > 315$ MeV), comparing 1D, NM and 3D distributions. The error bars (not shown) on the NM points are about a factor 1.8 bigger than those shown on the 3D points.

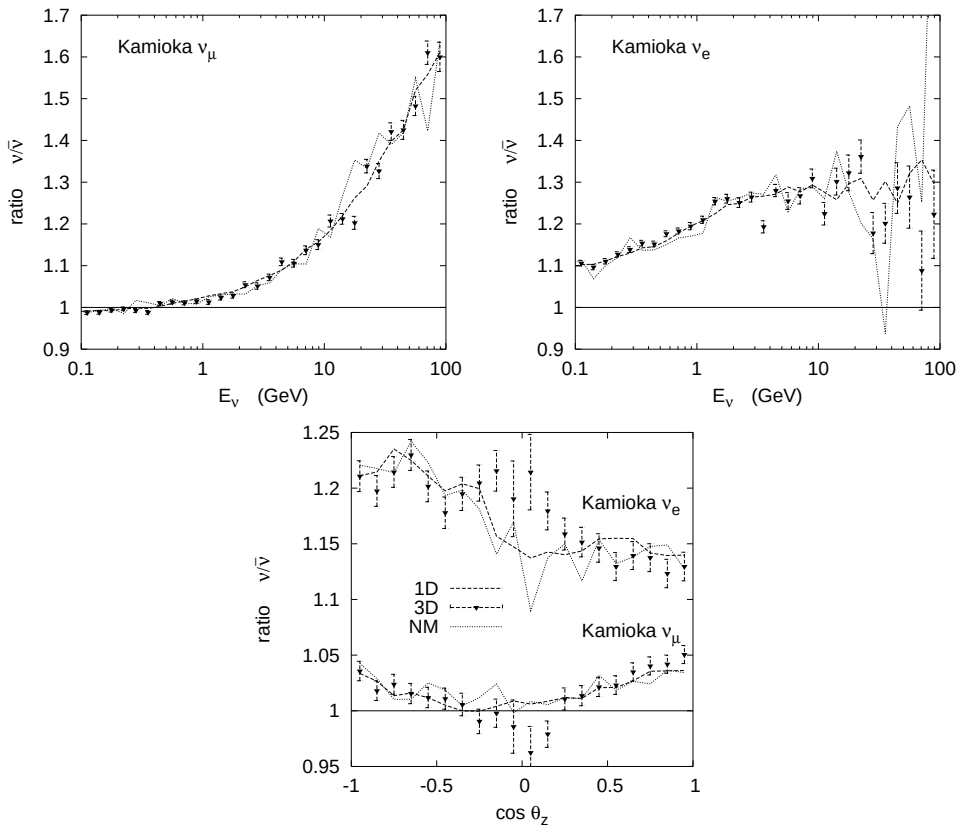

Figure 5: Neutrino to antineutrino ratios as a function of energy for (a) muon type neutrinos and (b) electron type neutrinos. (c) Zenith angle dependence of the neutrino to antineutrino ratios.

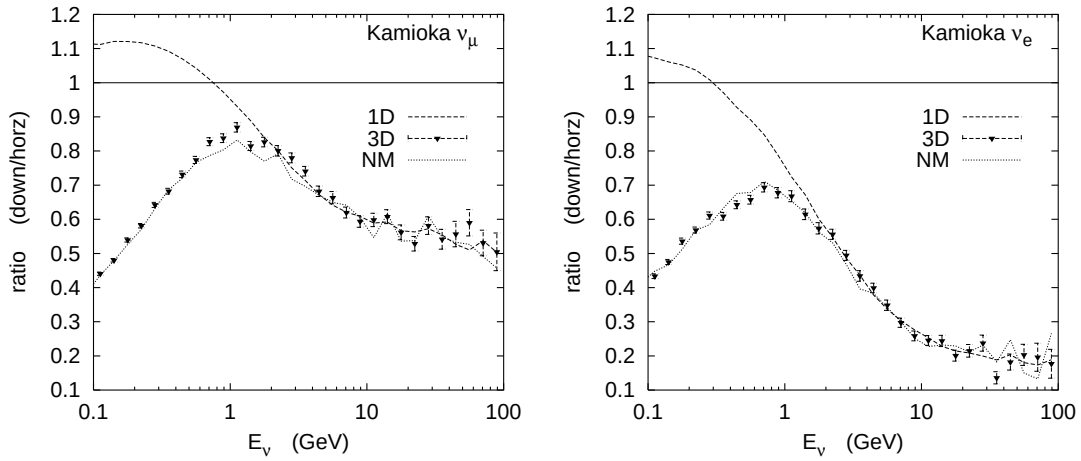

Figure 6: Ratio of downward to horizontal neutrino fluxes (a) muon neutrino type and (b) electron neutrino type.

an increasing role in the production at higher energies. There are no changes in these ratios between the 1D and 3D methods except for a possible slight excess in the 3D above statistics near the horizon in the electron neutrino ratio. This is inconsistent with the much larger effect shown by Wentz et. al [11]. Figures 6 and 7 show the down to horizontal ($R_{\rm DH}$) and up to down ($R_{\rm UD}$) ratios respectively (each of down, horizontal and up fluxes are taken in an interval of 0.4 in $\cos(\theta_z)$). $R_{\rm DH}$ deviates significantly between 1D and 3D at low energy due to the geometric effect, as seen earlier on figure 3. A conservative limit above which 3D effects can safely ignored in calculating this ratio is 5 GeV. The NM agrees with the 3D. The up-down ratios are consistent between 1D, NM and 3D at all energies. The change in the ratio with energy is governed by the difference in geomagnetic cutoff, which is locally very high at the Kamioka site and low at northern sites such as Soudan.

3.2 Azimuthal distributions

The azimuthal distributions of neutrinos are distorted by the curvature of their charged ancestors in the geomagnetic field. Effects are most important for primary cosmic rays and for the long-lived protons and muons in the atmosphere. As a consequence, the East-West asymmetry is different in the results of a 3D calculation as compared to the 1D results.

The ratio of neutrino to anti-neutrino fluxes is shown as a function of the azimuthal direction φ in figure 8 for electron-like neutrinos (left) and muon-like neutrinos (right), for the 1D, 3D and NM calculations. We have defined φ such that 0° is for neutrinos arriving from the North, 90° for neutrinos from the East and so on. The plots were made for neutrino energies above 315 MeV. We divide neutrino by anti-neutrino fluxes so that anisotropies resulting from the primary cutoffs should largely cancel. This plot therefore displays anisotropies primarily due to particle transport through the atmosphere. The 1D and 3D calculations differ strongly in these residual azimuthal anisotropies. The NM

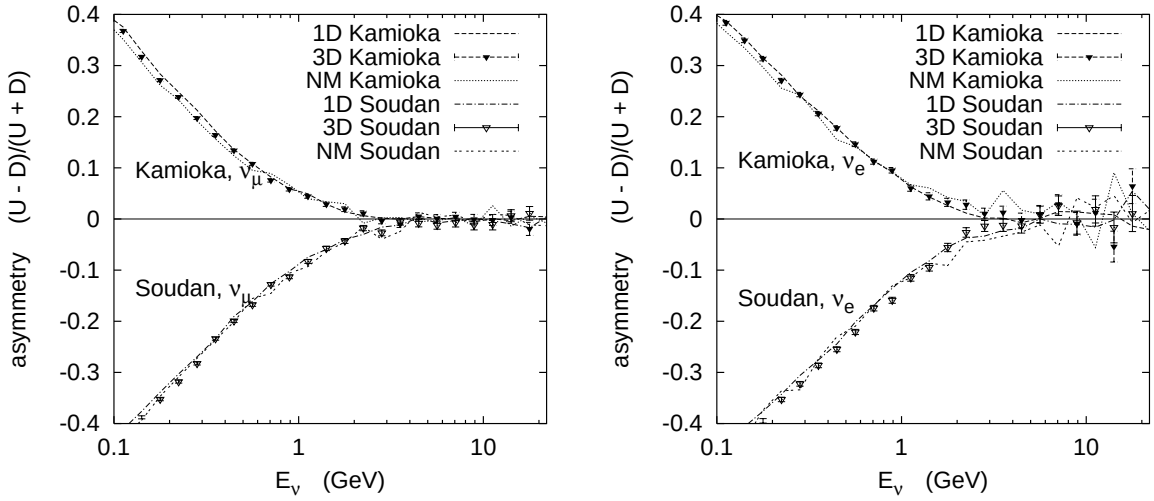

Figure 7: Ratio of upward to downward neutrino fluxes as a function of neutrino energy plotted as an asymmetry for both the Kamioka and Soudan sites. (a) muon neutrino type and (b) electron neutrino type.

calculation agrees with the 1D result, indicating that these differences are due to the bending of particles (mostly the muons) in the atmosphere.

The size of the East-West asymmetry $(E - W)/(E + W)$ for horizontal neutrinos ($|\cos\theta_z| < 0.5$) is shown in figure 9 as a function of neutrino energy for the 3D (points) and 1D (lines) calculations. East: $40° < \varphi < 140°$, West: $220° < \varphi < 320°$. In this figure each of the 1D lines agree well with each other, showing that the East-West effect is the same for all neutrino types. This is a consequence of the primary cutoff, which is the same for all neutrino types and the only source of azimuthal anisotropies in the 1D calculation. The shape of the 1D distributions is governed by the primary cutoff – at low neutrino energies the strength of the cutoffs is at a maximum, resulting in the maximum East-West asymmetry; as the neutrino energy rises, so the size of the asymmetry decreases as the primary cutoffs become progressively less important.

The points in figure 9 show that, for low energy neutrinos, the East-West asymmetry is much smaller for the 3D calculation; the NM results (not shown) also agree with this. This is because the correlation between the neutrino and primary directions decreases with decreasing neutrino energy, which is also related to the 3D geometrical effect. Thus, for low energy neutrinos the need for a fully 3D calculation is clear; however, even at higher neutrino energies the 1D and 3D results do not agree. Both the bending of primary particles (between injection and interaction) and muons is important to the East-West effect. Whereas the bending of protons produces the same result for all neutrino types (it is an extension of the cutoffs) the bending of muons introduces anti-particle/particle differences. The effect due to muons is simply a result of positive and negative muons bending in opposite directions in the geomagnetic field, resulting in an enhanced East-West asymmetry for the decay products of positive muons (ν_e and $\bar{\nu_\mu}$) as shown in figure 9.

The most important conclusion to draw from figure 9 is that the East-West asymmetry

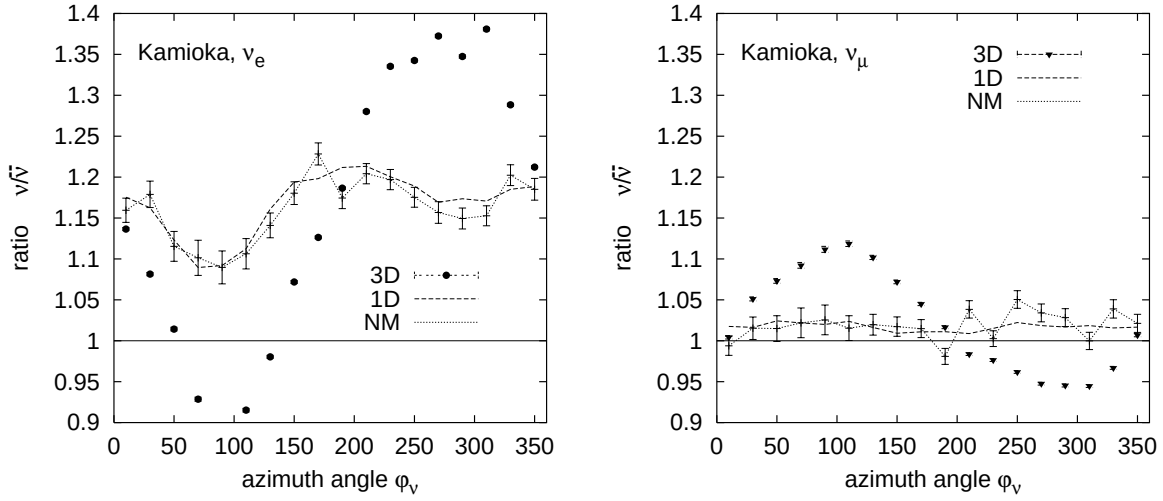

Figure 8: Neutrino to anti-neutrino flux ratios as a function of azimuthal angle at Kamioka, for electron-like (left) and muon-like (right) neutrinos. Points: 3D calculation; dashed line: 1D calculation; dotted line (with error bars): NM calculation (3D with the magnetic field neglected for particle transport in the atmosphere).

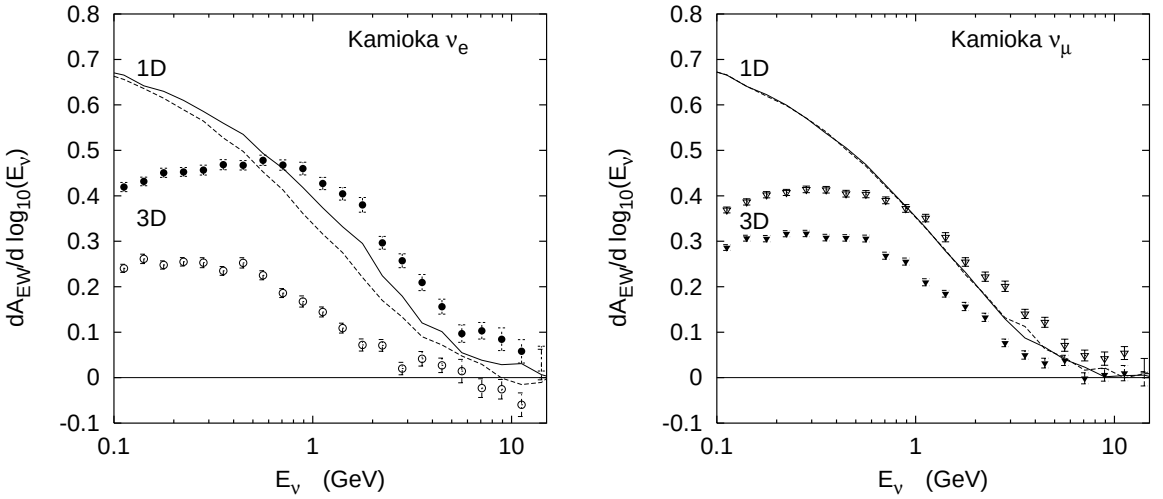

Figure 9: The size of the East-West asymmetry ($A_{EW} = (E-W)/(E+W)$) as a function of neutrino energy for the four neutrino species: ν_e (left, circles), ν_μ (right, triangles); neutrinos (filled, continuous line), anti-neutrinos (empty, dashed line). The lines show the results of the 1D calculation and the data points the 3D calculation.

is different in the 3D and 1D calculations even for 10 GeV neutrinos, and that the size of this effect is dependent on the neutrino type.

3.3 Path length distributions

The path length of the neutrinos from their production point to the place where they are detected is an important consideration when determining the neutrino oscillation parameters. A difference is expected between 1D and 3D calculations near the horizon. In the 1D calculation the only way of producing a horizontal neutrino is by the interaction of a primary which grazes the atmosphere and (because of the angle of incidence) interacts very high up. In the 3D simulation, there is the possibility that a horizontal neutrino may be produced from a more vertical cascade with a neutrino emitted sideways – such neutrinos are generally produced closer to the detector. This is illustrated in figure 10 which shows the distance distribution for neutrinos produced vertically and near the horizon with the 3D and 1D distributions superimposed on the same plot. The vertical distributions are nearly the same for 1D and 3D calculations whereas the horizontal distributions have an additional component in the 3D calculation at low path length (corresponding to horizontal neutrinos being produced from more vertical cascades). The mean path length is shown as a function of zenith angle in figure 11. For upward going neutrinos, the path length in the Earth ($2R_{\oplus}|\cos\theta_z|$) must be added.

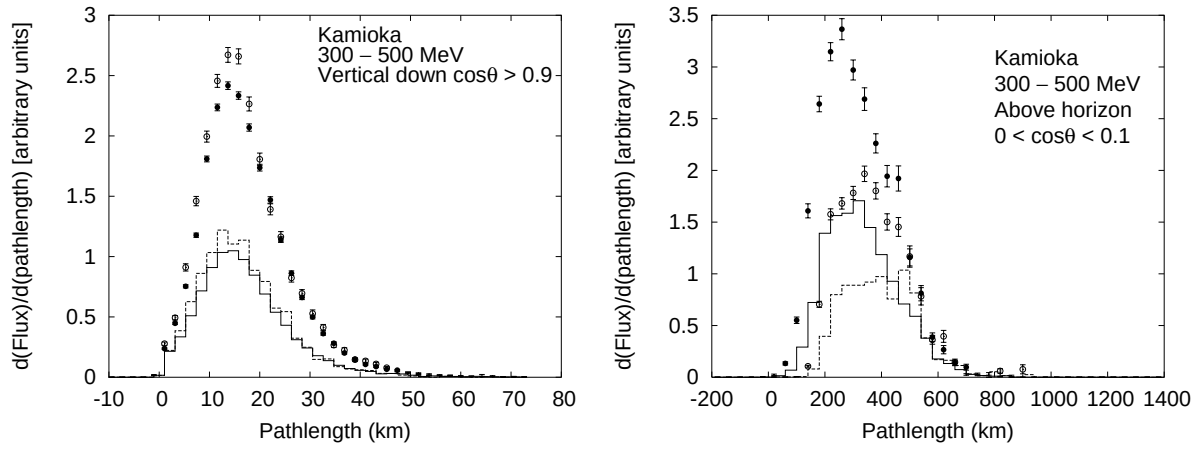

Figure 10: Distributions of neutrino path length from production to detection for vertically downward neutrinos (left) and near-horizontal neutrinos (right). Full (open) circles are muon neutrinos from the 3-D (1-D) calculation, and full (dashed) histograms are electron neutrinos from the 3-D (1-D) calculation.

The geometrical effect in the 3D calculation which causes the enhancement in the flux near the horizon also causes the mean production distance to be reduced. The reduction is 15% at the horizon for neutrinos with energies in the range 300-500 MeV, and quickly diminishes (2% in the $0.4 < \cos\theta_z < 0.5$ bin). At higher energy also, the effect diminishes: the path length reduction at the horizon is 4% for neutrinos above 1 GeV. Note that changing the altitude of the detector (see following section) has a similar sized effect on

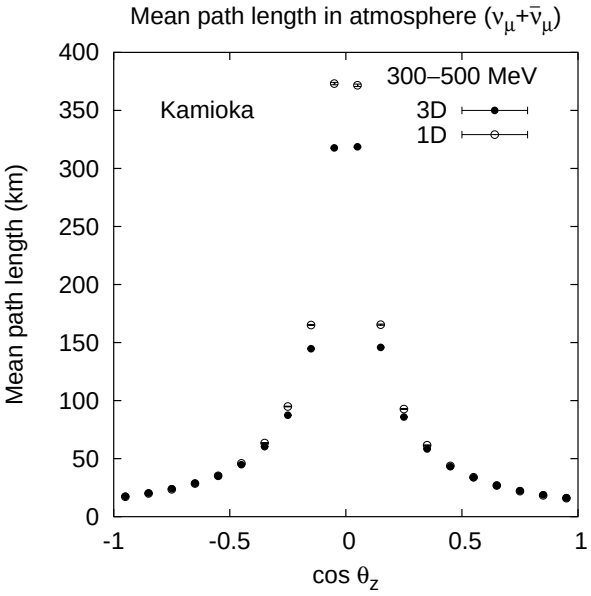

Figure 11: Mean path length distance in the atmosphere of muon neutrinos and antineutrinos in the range 300–500MeV as a function of zenith angle, comparing 3-D and 1-D calculations. For upward going neutrinos, the path length in the Earth must be added.

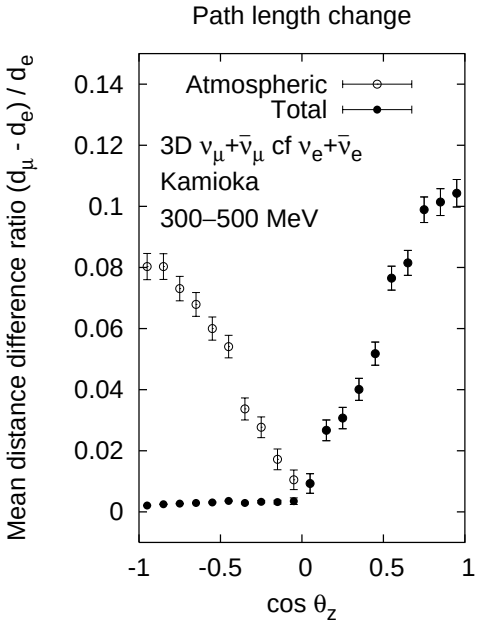

Figure 12: Comparison of the path lengths of electron and muon type neutrinos as a function of zenith angle. Full circles compare the total distances traveled (Earth + atmosphere) and open circles compare the distance traveled in the atmosphere only.

the path length distribution, it is important that the true altitude of the detector is used and not just an assumption that it is at sea level.

Figure 12 compares the path length distribution for electron and muon type neutrinos. Since the majority of electron neutrinos are produced in muon decay while most muon neutrinos are associated with muon *production*, muon neutrinos are produced on average higher in the atmosphere - this effect is only important for downward, nearly vertical neutrinos.

3.4 Detector size

An important technical question for a 3D calculation is, How large can the "detector" be without distorting the results? Since the geomagnetic cut-offs change rapidly at small geomagnetic latitudes, such as in Japan, the adoption of a large neutrino detector can, in principle, lead to incorrect predictions of the atmospheric neutrino flux at such locations. To study this uncertainty, we have repeated the calculation moving the detector away from its real location.

Our 3D calculation uses a circular detector of radius 500 km. We study the flux obtained by positioning the detector in steps of 500 km North, South, East and West from the real experimental location. Note that these displaced runs have a factor 10 lower Monte-Carlo statistics than the main runs. Figure 13 shows the zenith angle distribution of the flux of 300–500 MeV neutrinos for various distances away from Kamioka in increments of 500km from 2000km south to 2000km north. The flux varies by a factor of 3 over the range explored. Furthermore, the shape of the zenith angle distribution changes considerably over this range. Note the region in the upward direction ($\cos(\theta_Z)$ between -0.9 and -0.5) where the variation of flux with latitude reverses compared to the rest of the distribution. Such variations are to be expected because the cutoffs change considerably as a function of latitude.

As the neutrino energy increases, the variation decreases somewhat. In the neutrino energy range 0.5 – 1 GeV, the variation is about a factor 2.3 near the horizon. The second panel in figure 13 shows the distributions for the neutrino energy range 1 – 1.5 GeV where the variation over the $\pm$2000 km range studied is still about a factor of 2. For neutrino energies above 2 GeV, the variation is considerably smaller – about 20%.

The variations in the east-west direction are far less. This is expected since we are moving in a direction where the geomagnetic latitude doesn't change so rapidly. The fluxes vary by less than 10% over the 4000 km range studied in the 300 – 500 MeV neutrino energy range. The flux is not entirely flat in this direction since the direction of constant geomagnetic latitude is not exactly aligned with the East-West direction and because the field is not exactly a dipole.

The zenith angle distribution at SNO is shown in figure 14; the variations are considerably smaller than at Kamioka. Tserkovnyak et al [17] reported a 'cliff' effect in the geomagnetic cutoffs near the SNO site; this can be seen in the downward fluxes on figure 14 – moving north from SNO causes a tiny ($< 5\%$) variation, whereas moving south causes a 20% variation in the fluxes. The reason the effect on the fluxes is considerably less at SNO than at Kamioka is because the cutoffs at Kamioka are close to 20 GeV which is the most important primary energy for the production of neutrinos of these low energies;

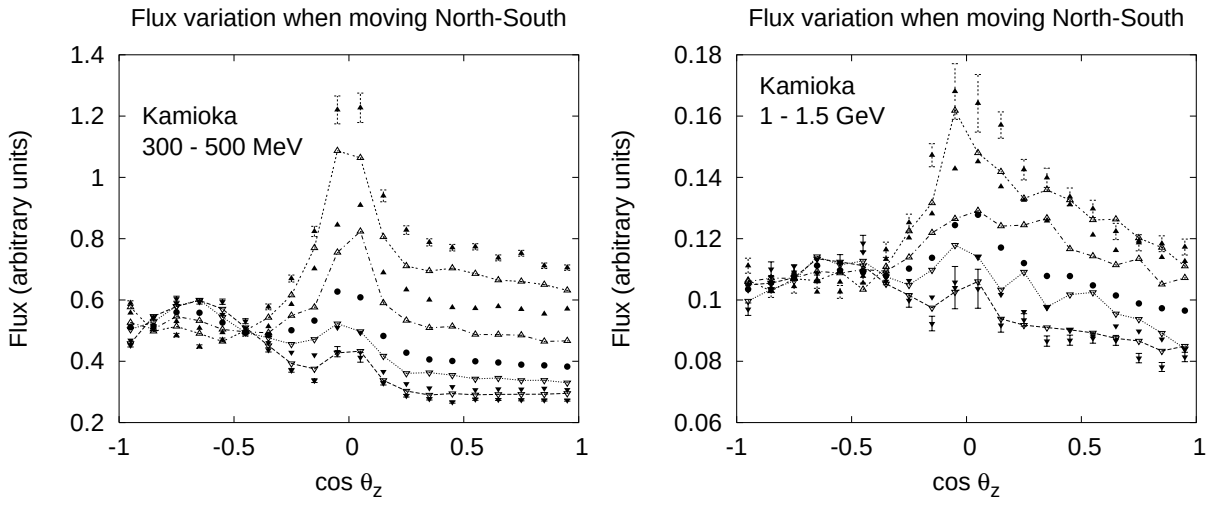

Figure 13: Results of runs spaced 500 km apart in latitude. The solid circles are at the Kamioka site, upward triangles are for runs going north from the detector site (alternating full and open symbols) and downward triangles are for runs going south. The lines are shown to guide the eye by joining the points on every second curve (at ±500km and ±1500 km). Apart from the run at the Kamioka site, statistics are the same for all runs and error bars are shown as examples on the points at ±2000 km. Statistics on the Kamioka site points are a factor 10 larger. Left panel: neutrinos in the energy range 300 – 500 MeV. Right panel: neutrinos in the energy range 1 – 1.5 GeV.

any change in the cutoffs has a dramatic effect on the fluxes. At SNO, however, which is much closer to the geomagnetic poles, the vertical cutoffs are around 2 GeV. Since this is below the main primary energy range for neutrino production, the effect as a function of latitude is smaller. The east-west variation around the SNO site is also minimal, in much the same way as at Kamioka. These conclusions are also valid for the Soudan detector site which is only 1.4° (150 km) north and 11° (840 km) west of SNO.

To determine what detector size is appropriate for use in a flux calculation, the functional form of the flux variation with both latitude and longitude is studied in each zenith angle bin separately. If the flux variation is linear within the range used for a simulated detector (and the simulated detector is centered on the real detector location), then the average flux across the simulated detector will be equal to the flux at the center of the detector. Any non-linear variation however will result in a difference in fluxes. If the flux is parameterized using a quadratic $\phi(x) = A_0 + A_1 x + A_2 x^2$, where x is the distance as measured from the detector center, then the correction C for using a large rectangular detector (from $x = -\Delta$ to $x = +\Delta$) in the simulation is

$$C = \frac{\frac{1}{2\Delta}\int_{-\Delta}^{+\Delta}\phi(x)\mathrm{d}x - \phi(0)}{\phi(0)} = \frac{A_2\Delta^2}{3A_0} \tag{2}$$

The corresponding expression for a circular (or elliptical) detector shape of radius r is $C = A_2 r^2/4A_0$.

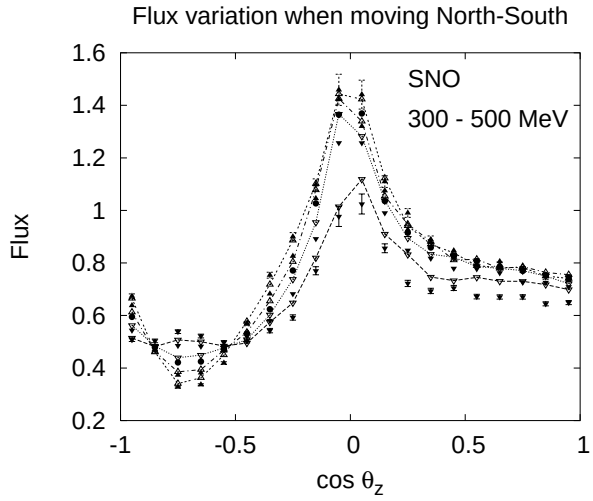

Figure 14: Results of runs spaced 500 km apart in latitude for neutrinos in the energy range 300 – 500 MeV around the SNO location. The legend is the same as in figure 13

Quadratic fits to the variation in each zenith angle bin are made to determine the values of A_2/A_0 for use in the expression given in equation 2. The resulting corrections C are shown in figure 15 for neutrino energies 300 – 500 MeV. Since the expressions for C vary only by a scale factor proportional to the detector size squared, these numbers can be scaled to any detector size. The North-South corrections at Kamioka are the largest; with a $\Delta = 2000$ km detector C is about 10%. With the detector size used in this paper ($r = 500$ km, shown on the right hand scale of figure 15) C remains below 0.5% for all zenith angle bins. Figure 15 also shows C for the North-South variation at SNO (of opposite sign to the Kamioka correction to correct for the 'cliff' effect) and the East-West correction at Kamioka (which is considerably smaller than the North-South variation. The East-West variation at SNO (not shown) is also negligible (i.e. $C < 0.5\%$ for a 2000 km detector). Similar curves have also been made for higher energies. The corrections show similar features to those illustrated but with diminishing size as the energy increases. The average C for downward fluxes at Kamioka (SNO) is 5.1% (-1.1%) $\pm$0.3% in the energy range 0.5 – 1 GeV and 1.5% (-0.2%) $\pm$0.5% in the energy range 1 – 1.5 GeV. At higher energies, C becomes negligible.

In summary, the investigation of the variation of the calculated neutrino fluxes with latitude has revealed large variations, particularly at Kamioka where the variation in local cutoffs affects the most important energy range of cosmic rays for low energy neutrino production. These variations indicate that caution should be used in deciding how much to extend the size of the detector in a 3D calculation. The present calculation uses a detector which is circular of radius $r = 500$ km which is sufficiently small to keep corrections less than 0.5%. We elect to keep this detector size and not to make any correction on the data – possibly in the future, we will use an elliptical detector with $r = 500$ km in the North-South direction and larger in the East-West direction.

Variations in the altitude of the detector have also been studied. An increase of the

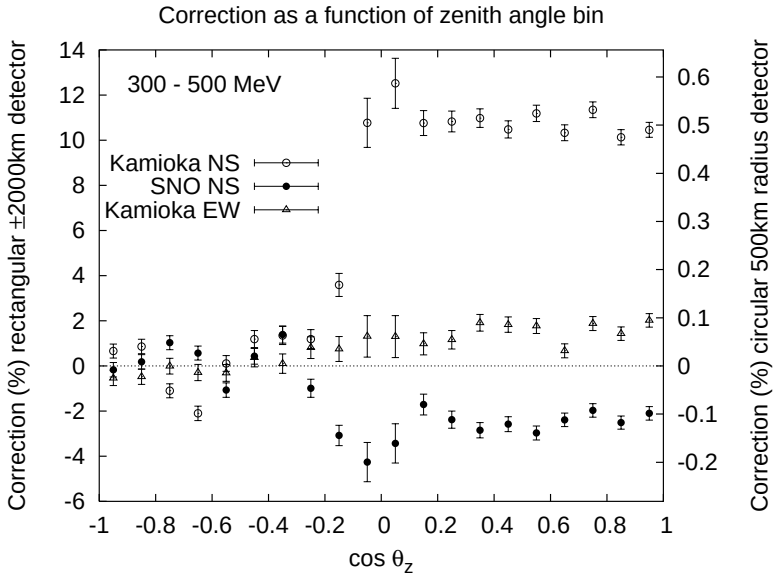

Figure 15: Plot of the correction to be applied to the fluxes if a large detector is used in the calculations. The left scale gives the size of correction for a rectangular detector with extent ±2000 km about the Kamioka site and the right scale gives the correction for a circular (or elliptical) detector with radius 500 km.

geometrical 3D enhancement near the horizon (5% per kilometre rise in altitude for 300 to 500 MeV neutrinos) is observed, as expected [9] since the detector is moved closer towards the production altitude.

4 Conclusions

We have extended the 1-dimensional neutrino flux calculation [1, 2] to three dimensions. We compare results of the 3D and 1D calculations for neutrino energies from 100 MeV to 10 GeV over the full 4π solid angle. Results are given for Kamioka, which is at low geomagnetic latitude, and for SNO and Soudan at high latitude.

The angle-averaged fluxes are identical within statistics for $E_\nu > 1$ GeV, with approximately a 3% excess in the 3D calculation for sub-GeV neutrinos. The differences are much more noticeable in the zenith angle distributions for $E_\nu < 1$ GeV, which show a significant excess in the 3D calculation for $-0.1 < \cos\theta < 0.1$ and a smaller deficit for $|\cos\theta| > 0.4$. The differences largely cancel in the angular integral, leaving the small (3%) overall difference mentioned above. The zenith-angle differences decrease with energy and become completely negligible for $E_\nu > 5$ GeV.

Corresponding to the horizontal excess in the 3D calculation is a contribution to the path length distribution of near horizontal neutrinos which reduces the average path length for horizontal neutrinos with $300 < E_\nu < 500$ MeV by 15% relative to the 1D calculation. The corresponding reduction decreases to 4% for $E_\nu > 1$ GeV. This difference could have a small effect on the inferred neutrino mass squared difference (Δm^2), but this remains

to be determined.

The angle-integrated neutrino flavor ratio, calculated as $(\nu_\mu + \frac{1}{2}\overline{\nu}_\mu) / (\nu_e + \frac{1}{2}\overline{\nu}_e)$ is the same in the 3D as in the 1D calculation. The $\langle\nu\rangle / \langle\overline{\nu}\rangle$ ratio (where $\langle ...\rangle$ indicates angle averaging) is also the same. The ratio of downward to upward neutrinos ($\cos\theta > 0.4$ and $\cos\theta < -0.4$) are nearly identical in the 3D and 1D calculations. However the ratio of downward to horizontal fluxes changes considerably below 1 GeV when moving to a 3D calculation. Because the neutrino flavor ratio and the up-down ratio are the most important quantities for determining the neutrino oscillation parameter $\sin\theta_{23}$, we do not expect correct treatment of the 3D effects in itself to lead to a large change in inferred value of this parameter. The oscillation parameter Δm^2_{23} however is also sensitive to the down-horizontal ratio and 3D effects could possibly lead to a change in this parameter, particularly if low energy horizontal neutrinos are used in the analysis.

The azimuthal distributions in the 3D calculation show interesting effects which depend on neutrino flavor and also distinguish between neutrinos and anti-neutrinos. These differences arise from bending of charged particles inside the atmosphere. Unlike enhancement of low-energy neutrinos near the horizon (which is a geometrical effect) this geomagnetic effect persists to higher energy. Because of its $\nu - \bar{\nu}$-dependence, this generalized East-West effect could be detectable in a sufficiently large detector with the capability of determining the sign of neutrino-induced leptons. Because $\sigma_\nu > \sigma_{\bar{\nu}}$ for both neutrino flavors while the relation between muon charge and the lepton number of its neutrino decay product is opposite for ν_e and ν_μ, this effect may also be visible as a difference in the East-West effect for electron-like and muon-like events [15].

We have shown that the treatment near the horizon in a 3D calculation requires special consideration, in particular in handling the weighting when a flat detector is used. Computational speed is a major concern in a 3-D calculation. The detector may be made artificially large to average the neutrino flux over a larger area around the detector site. We investigated of variation of the flux with distance from the detector site and find that the changes are dramatic. However, the variation of the flux remains linear for a significant distance and the use of a detector with an extent of the order of 1000km may be used with care. The problems are largest when moving in a North-South direction at a detector located at low geomagnetic latitudes (e.g. Kamioka).

In a forthcoming paper we will consider the 3D flux for different assumptions about the primary spectrum. We expect the limiting factors in the knowledge of neutrino fluxes (at production, before oscillations) to be uncertainties in the primary spectrum and in the treatment of hadronic interactions, rather than 3D effects.

Acknowledgements

The work of TKG and TS is supported in part by the U.S. Department of Energy under DE-FG02 91ER 40626. One of the authors (SR) is supported by a PPARC studentship.

References

[1] G. Barr, T.K. Gaisser & T. Stanev, Phys. Rev. D **39**, 3532 (1989).

[2] V. Agrawal, P. Lipari, T.K. Gaisser & T. Stanev, Phys. Rev. D **53**, 1314 (1996).

[3] K.S. Hirata *et al.*, Phys. Lett. B**205**, 416 (1988); Phys. Lett. B**280**, 146 (1992).

[4] D. Casper *et al.*, Phys. Rev.Lett. **66**, 2561 (1991); R. Becker-Szendi *et al.*, Phys. Rev. D **46**, 3720 (1992).

[5] Y. Fukuda *et al.*, Phys. Rev. Lett. **81**, 1562 (1998).

[6] M. Sanchez *et al.*, Phys. Rev. D **68**, 113004 (2003).

[7] M. Ambrosio *et al.*, Phys. Lett. B **517**, 59 (2001).

[8] T. Kajita & Y. Totsuka, Rev. Mod. Phys. **73**, 85 (2001).

[9] P. Lipari, Astropart. Phys. **14**, 153 (2000).

[10] T. K. Gaisser & M. Honda, Ann. Rev. Nucl. Part. Sci. **52**, 153 (2002) [arXiv:hep-ph/0203272].

[11] J. Wentz, Phys. Rev. D**67**, 073020 (2003).

[12] G. Battistoni *et al.*, Astropart. Phys. **12**, 315 (2000).

[13] G. Battistoni *et al.*, astro-ph/0207035

[14] A. Fasso *et al.*, invited talk in the Proceedings of the MonteCarlo 2000 Conference, Lisbon; see: http://www.fluka.org

[15] P. Lipari Astropart. Phys. **14**, 171 (2000).

[16] M. Honda, T. Kajita, K. Kasahara and S. Midorikawa, Phys. Rev. D **64**, 053011 (2001) [arXiv:hep-ph/0103328].

[17] Y. Tserkovnyak *et al.*, Astropart. Phys. **18**, 449 (2003).

[18] D. Heck *et al.*, Forschungszentrum Karlsruhe, FZKA Report No. 6019 (1998).

[19] Y. Liu, L. Derome and M. Buénerd Phys. Rev. D **67**, 073022 (2003).

[20] V. Plyaskin, Phys. Lett. B**516**, 213 (2001).

[21] J. Favier, R. Kossakowski and J.P. Vialle, Phys. Rev. D **68**, 093006 (2003); see also M. Aquilar *et al.* (AMS Collaboration), Physics Reports **366**, 331 (2002).

[22] J. Alcaraz *et al.*, Phys. Lett. B**472**, 215 (2000).

[23] http://nssdc.gsfc.nasa.gov/space/model/models/igrf.html

[24] P. Zuccon *et al.*, Astropart. Phys. **20**, 221 (2004).

[25] R. Engel *et al.*, Proc. 27th ICRC, Hamburg, 1381 (2001).

[26] J. Alcaraz *et al.*, Phys. Lett. B**490**, 27 (2000).

[27] J.Z. Wang *et al.*, Ap. J. **564**, 244 (2002).

[28] M. Boezio *et al.*, Astropart. Phys. **19**, 583 (2003).

[29] G. Barr *et al.*, Proc. 28th ICRC, Tsukuba, 1423 (2003).